Drug delivery and antimicrobial studies of chitosan-alginate based hydroxyapatite bioscaffolds formed by the Casein micelle assisted synthesis

Jariya, S. A.Iynoon; Padmanabhan, Varun Prasath; Kulandaivelu, Ravichandran; Prakash, Natarajan; Mohammad, Faruq; Al-Lohedan, Hamad A.; Paiman, Suriati; Schirhagl, Romana; Hossain, M. A.Motalib; Sagadevan, Suresh

Published in:
Materials Chemistry and Physics

DOI:
10.1016/j.matchemphys.2021.125019

Publication date:
2021

Materials Chemistry and Physics 272 (2021) 125019

Contents lists available at ScienceDirect

Materials Chemistry and Physics

journal homepage: www.elsevier.com/locate/matchemphys

Drug delivery and antimicrobial studies of chitosan-alginate based hydroxyapatite bioscaffolds formed by the Casein micelle assisted synthesis

S.A. Iynoon Jariya [a], Varun Prasath Padmanabhan [a], Ravichandran Kulandaivelu [a,**], Natarajan Prakash [b], Faruq Mohammad [c], Hamad A. Al-Lohedan [c], Suriati Paiman [d], Romana Schirhagl [e], M.A. Motalib Hossain [f], Suresh Sagadevan [f,*]

[a] Department of Analytical Chemistry, University of Madras, Guindy Campus, Chennai, 25, India
[b] Department of Chemistry, Saveetha School of Engineering, SIMATS, Saveetha University, Chennai-602 105, India
[c] Department of Chemistry, College of Science, King Saud University, P.O. Box 2455, Riyadh, 11451, Saudi Arabia
[d] Department of Physics, Faculty of Science, Universiti Putra Malaysia, 43400, UPM Serdang, Selangor, Malaysia
[e] Groningen University, University Medical Center Groningen, Antonius Deusinglaan 1, 9713, AW Groningen, Netherlands
[f] Nanotechnology & Catalysis Research Centre, University of Malaya, Kuala Lumpur, 50603, Malaysia

HIGHLIGHTS

- Developed a novel chitosan-alginate containing fluorine substituted hydroxyapatite composite.
- Alginate presence in the scaffold caused 88.78% porous and 67.5% biodegradation capacity.
- Availability of chitosan in the composite supported for the controlled drug release.
- Hydroxyapatite to offer efficient antibacterial and antifungal characteristics to the composite.

ARTICLE INFO

Keywords:
Casein micelle
Hydroxyapatite
Ciprofloxacin drug release
Chitosan-alginate matrices
Bioactivity and biodegradability

ABSTRACT

The present study aims to develop a hydroxyapatite (HAP) based scaffold composite for orthopaedic applications and for that, we adopt a Casein (Cs) micelle assisted synthesis route for the formation of a composite. Following the synthesis and characterization of various fluorine (2% and 5%) substituted HAPs (FHAP), they have been tested for the release of Ciprofloxacin (CIP) drug and antimicrobial efficacy. The physicochemical characterization such as FTIR and Raman confirms the successful formation of the HAP composites. Similarly, the powder XRD and FESEM analysis have used for the confirmation of crystallinity and morphological behaviour, respectively. The elemental composition has confirmed using EDX analysis. The antimicrobial studies indicate that the 5% FHAP sample is possessing superior antifungal and antibacterial activities and the highest activity has been observed against the gram-positive bacteria (*Staphylococcus aureus*) with an inhibition zone of 47 mm while the gram-negative bacteria (*Escherichia coli)* has only 38 mm inhibition zone. The CIP drug release profile has been controlling with the Cs/5% FHAP sample. Therefore, this composite has carried out for the scaffold formation with the use of chitosan-alginate matrices. Further, characterization of chitosan-alginate/5% FHAP scaffold composite indicates porous, biodegradable, considerable water uptake and retention ability, along with the maintenance of controlled CIP drug-releasing properties. Based on the analysis, the as-synthesized chitosan-alginate/5% FHAP scaffold composite can be suitable for the biomedical and bioengineering applications of bone tissue growth and as an implant.

* Corresponding author.
** Corresponding author.
E-mail addresses: raavees@gmail.com (R. Kulandaivelu), drsureshnano@gmail.com (S. Sagadevan).

https://doi.org/10.1016/j.matchemphys.2021.125019
Received 10 May 2021; Received in revised form 9 July 2021; Accepted 12 July 2021
Available online 13 July 2021

1. Introduction

In recent years, the increased interest in nanocomposites manufactured from polymers, ceramics, and metals for biomedical engineering applications of joints replacement and other body parts in the field of orthopaedics were due to the mechanical resistance and enhanced biocompatibility, in addition to non-toxicity [1–5]. Among various kinds of nano/biocomposites applicable to the biomedical sector, the ceramic materials containing the Ca and P elements had been a special role towards the development of orthopaedic and dental implants where it served as an abundant component in the bones, teeth, pathological atherosclerotic lesions, urinary calculus, and calcification of tissues in the invertebrates [6–9]. Hydroxyapatite (HAP) was observed to be highly biocompatible and non-toxic with the maintenance of excellent osteointegrative and osteoconduction characteristics [10–15]. In this context, the HAP was formed in its nanosized, which had drawn a special attention as metal implants and bone tissues for frequent use in orthopaedic surgery [16–19]. Since the synthesis of nanosized HAP with the involvement of natural agents such as surfactants, polymers, and gums [20–27] for the formation of soft template could be fabricated using the wet chemical routes [28] like sol-gel [29], mechanochemical [30], hydrothermal [31], microwave heating [32], microemulsion [33], and template addition [34]. The incorporation of surfactants or polymers during the synthesis, controls the particle's size from getting into agglomeration and thereby making the synthesis procedure to be more flexible, convenient, and tailored for the effective synthesis of nano-level HAP particles [35,36]. Besides those techniques, the formation of nano HAP by the other conventional route involved the natural agents, sintering aided polymer encapsulated core-shell. HAP was used as a drug delivery vehicle for the controlled release applications. As an example, polymeric gum was one of the naturally occurring acacia plant exudates which was rich in polysaccharides and glycoproteins. In addition, this plant gum also contained arabinopyranose, galactopyranose, rhamnopyranose, arabinofuranose, glucopyranosyl uronic acid, 4-O methyl glucopyranosyl uronic acid, and a small amount of hydroxyproline-rich protein [37–40]. Of various components present in the natural gum, arabinogalactan was the major component and when used as a surfactant, it can easily get attached to the proteins and functions as a signalling molecule. The other advantages of this component were the emulsifying agent and as an additive in the food industry and thereby confirming as a safe, biocompatible, and effective drug delivery vehicle for the HAP-based composites [21,22].

Therefore, considering the advantages of natural gum and the role played by HAP as a drug-delivering agent, the present study aims to develop a sustainable drug-carrying system consisting of a chitosan-alginate FHAP scaffold. In this, we carried out the synthesis, characterization, drug release, and biological activity of Casein (Cs) assisted Fluorine substituted HAP (Cs-FHAP) nanocomposite, which have been used to produce chitosan-alginate FHAP scaffold.

2. Materials and methods

Calcium nitrate tetrahydrate ($CaNO_3{\cdot}4H_2O$), Ammonium dihydrogen phosphate ($NH_4H_2PO_4$), Ammonium fluoride (NH_4F), Ethanol, and Cs were purchased from Sigma Aldrich Chemicals. Pure hydroxyapatite (HAP), Fluoride substituted hydroxyapatite (FHAP) and Cs-assisted fluoride substituted nano-hydroxyapatite (Cs-FHAP) were synthesized by the sol-gel approach. Analytical grade solvents and double distilled (DD) water were used for synthesis and purification.

$$mCa(NO_3)_2 + 6NH_4H_2PO_4 + yNH_4F + xNH_4OH \rightarrow Ca_m(PO_4)_6(OH)_{x\text{-}y}F_y + NH_4NO_3 + H_2O$$

2.1. Synthesis of Cs-FHAP

For the preparation of Cs-FHAP, we used an ethanolic solution of calcium nitrate and adjusted its pH to 11 using the concentrated ammonia solution, followed by the addition of 50 mg of Cs and heated at 60 °C using a magnetic stirrer. Similarly, a mixed solution of ammonium dihydrogen phosphate and ammonium fluoride were adjusted to the same pH using concentrated ammonia and added with the solution in a drop-wise manner. The solution mixture was heated at 85 °C and a white semi gelatinous precipitate was formed, which on vigorous stirring transformed into a gel (all over the synthesis period, the pH was maintained in the range of 10.5–11). Thus, produced gel was aged at room temperature for about 24 h and dryed in an air oven set at 110 °C overnight. The resulting FHAP product was sintered at 800 °C for 2 h in a muffle furnace and then allowed to cool in the furnace itself, so as to undergo the development of the HAP phase. Finally, the obtained product was grinded to powder using mortar and pestle. The same procedure was applied for the formation of pure HAP (used as a control) but without the inclusion of ammonium fluoride in the reaction mixture. The following experimental conditions (Table 1) are applied for the formation of various samples of HAP.

2.2. Preparation of chitosan–alginate/5% FHAP composite scaffolds

For the scaffold formation containing chitosan–alginate/FHAP composite, about 1 wt% (0.25 g) of chitosan was dissolved in 25 mL of 2% acetic acid, followed by the addition of 1 wt% (0.25 g) of sodium alginate. The mixture solution was stirred for 24 h to get a homogeneous mixture with no air bubbles. To this, 0.5 g of earlier prepared Cs-5% FHAP was added and stirred for 4 h to form a slurry. The final chitosan–alginate/FHAP blend ratio in the composite was set as 1:1. The slurry was transferred to a 24-well cell culture plate, cross-linked with 1% (w/v) $CaCl_2$ solution for 15 min, and finally immersed in distilled water for 24 h to remove any residual sodium acetate and unbound $CaCl_2$. Thus, obtained samples were stored in a freezer maintained at 15 °C until they become frozen and subsequently, the frozen samples were lyophilized in a freeze dryer for 48 h at −80 °C to obtain the dried samples of chitosan–alginate/5% FHAP composite scaffolds.

By making use of the same procedure, pure chitosan/5% FHAP composite scaffolds (as control) were synthesized without the addition of sodium alginate and calcium chloride in order to compare the change of biodegradability, porosity, water uptake, and retention studies.

2.3. In vitro bioactivity studies

The *in vitro* bioactivity tests were conducted for the prepared samples of pure HAP, FHAP, Cs-HAP, and chitosan-alginate/5% FHAP in simulated body fluid solution (SBF) where the solutions were prepared in accordance with Kokubo's protocol [41]. For the bioactivity, the testing samples prepared in the form of a pellet were first immersed in the SBF solution (at a ratio of 1 mg/mL) maintained at pH to 7.4 in sterilized bottles kept at 37 °C for 14 days. After the stipulated time, the soaked pellets were taken out, washed gently with deionized water, dried, and then analyzed for the extent of apatite formation at the surface using the FESEM technique.

Table 1
Concentration of components used for the formation of various HAP samples.

Sample	Ca $(NO_3)_2{\cdot}4H_2O$ (mol/L)	$NH_4H_2PO_4$ (mol/L)	NH_4F (mol/L)	Cs (mg)
Pure HAP	1.00	0.6	–	–
2% FHAP	1.00	0.6	0.064	–
5% FHAP	1.00	0.6	0.16	–
Cs-2% FHAP	1.00	0.6	0.064	50
Cs-5% FHAP	1.00	0.6	0.16	50

2.4. Studies of drug loading and release

Typically, 100 mg of Ciprofloxacin (CIP) drug and 100 mg either of HAP, 2% FHAP, 5% FHAP, Cs-2% FHAP, or Cs-5% FHAP crystals were dispersed in 100 mL of DD water. This mixed solution was stirred for about 24 h at room temperature. After this period, the precipitate was separated by centrifugation, dried, and the drug-loaded sample was collected in the form of a pellet. Now the bioceramic pellet having the CIP drug was placed into the Phosphate buffer solution (PBS; pH 7.4) and subjected to horizontal agitation on a shaking water bath at 37 °C. After each specified time interval, about 5 mL of the testing samples (containing the released drug) were collected and replaced with an equal amount of the fresh medium. Finally, the amount of CIP drug that got released into the medium at various time intervals was determined by UV–Vis spectroscopy. Also, the same procedure was repeated for the testing of chitosan-alginate/5% FHAP and other bioceramic samples.

2.5. Porosity measurements

To understand the porosity of as-synthesized scaffold samples (chitosan/5% FHAP and chitosan-alginate/5% FHAP) quantitatively, the liquid displacement technique was employed. Since, the scaffolds are insoluble in ethanol solvent and its easy penetrating ability into the scaffold pores protects from the occurrence of any shrinkage or swelling. For testing, a known weight (W) of the sample was immersed in a graduated cylinder containing a known volume (V_1) of ethanol solvent, and the evacuation followed by depressurization was performed for the undisturbed samples soaked in ethanol. In this process, the ethanol solvent gets diffused into the pores and can be repeated continuously until we see the air bubbles appearing to stop. At this stage, the volume of ethanol and ethanol-soaked scaffold was noted as V_2 and the difference in the two volumes (V_2–V_1) was measured. Further, the scaffold sample was removed from the cylinder that contains ethanol solvent to measure the residual volume (V_3) of ethanol and by making use of the following formula, the porosity was calculated [42].

$$\text{Porosity } (\varepsilon) = (V_1 - V_3)/(V_2 - V_3) \times 100 \quad (1)$$

2.6. Studies of water uptake and retention ability

To understand the water uptake and retention ability of as-synthesized scaffolds, the same procedure as similar to the porosity measurements was employed. For testing, weighed dry scaffold samples (W_1) and immersed them in the DD water for a period of 24 h and after that, the scaffolds were taken out and placed on a mesh. Now the disproportionate water drained from the scaffold sample was weighed (W_2) to determine the water uptake. Similarly, to investigate the water retention ability, the wet scaffolds were transferred to a centrifuge tube and subjected to centrifugation at 800 rpm for 5 min and immediately recorded the scaffold weight at this stage as (W'_2). By making use of the following formula, the percentage of water absorption (E_A) and water retention (E_R) of the scaffolds at equilibrium were calculated,

$$E_A = \frac{(W_2 - W_1)}{(W_1)} \times 100 \quad (2)$$

$$E_R = \frac{(W'_2 - W_1)}{(W_1)} \times 100 \quad (3)$$

2.7. In vitro biodegradation test

For the investigation of the scaffold's biodegradation ability *in vitro*, prepared a solution mixture (of 50 mL volume) containing 0.1 M PBS (made of sodium phosphate monobasic and sodium phosphate dibasic heptahydrate; pH 7.2) and lysozyme enzyme (0.5 mg/mL concentration). To this solution mixture, the weights (W_0) of synthesized samples, chitosan-5% FHAP and chitosan-alginate 5% FHAP were measured, immersed individually, and kept for the oscillation at 37.0 ± 0.5 °C. The samples after soaking for 21 days were removed, washed with deionized water, freeze-dried, and weighed again (W_1). The following formula was used to calculate the weight loss (W_L) of each sample,

$$W_L = \frac{(W_0 - W_1)}{(W_0)} \times 100\% \quad (4)$$

where, W_0 and W_1 denote the weights of scaffold samples before and after soaking in the solvent mixture, respectively, and for the accuracy of measurements, three parallel samples were used for the analysis.

2.8. Studies of antibacterial activity

The agar disc diffusion method that makes use of the Muller Hinton agar (MHA) medium was employed. For the antibacterial studies, the stock cultures were maintained at 4 °C. For the experiments, the active cultures were prepared by transferring a loop full of bacterial cells from the stock cultures to the test tubes of nutrient broth incubated at 37 °C for 24 h period.

About 3.8 g of Muller Hinton agar medium was weighed and dissolved in 100 mL of distilled water followed by the addition of 1 g of agar and kept the medium for sterilization. After the sterilization process, the media was transferred to sterile Petri plates and was allowed to solidify for 1 h and it gets solidified. The inoculums were spread on the solid plates with a sterile swab moistened with the bacterial suspension. The discs were prepared with 20 μL of samples (H1-pure HAP, H2–Cs-2% FHAP, and H3–Cs-5% FHAP) having the concentrations of 100 mg/mL, 20 μL each of DMSO as the negative control and streptomycin (1 mg/mL) as positive control placed on the MHA plates and were incubated at 37 °C for 24 h. Finally, the microbial growth was determined by measuring the diameter of the zone of inhibition (ZoI).

2.9. Studies of antifungal activity

As similar to the stock solutions and samples prepared for antibacterial activity, the same procedure was used for the preparation of stocks and cultures for the antifungal activity studies too. For the antifungal studies, the disc diffusion method on potato dextrose agar (PDA) medium was used by weighing about 4.4 g of the medium dissolved in 100 mL of distilled water followed by the addition of 1 g of agar and kept the medium for sterilization. The same process (antibacterial activity) of solidification of the medium, followed by the spreading of inoculums on the solid plates with a sterile swab moistened with the fungal suspension was employed. Also, the discs prepared with 20 μL samples (H1, H2, and H3) of 100 mg/mL concentration 20 μL of DMSO as a negative control, and 20 μL ketocanzole (20 μg) as a positive control were placed on the PDA plates, incubated at 37 °C for 24 h and finally measured the ZoI.

2.10. Instrumental analysis

The powder X-ray diffraction (XRD) reflection patterns for all the synthesized samples was performed using Rich Siefert 3000 diffractometer with $CuK_{\alpha 1}$ radiation (λ = 1.5406 Å). The Fourier transform infrared (FTIR) spectra for the surface functionality and bonding using Shimadzu FT-IR 8300 series instrument and Raman spectra were recorded on Raman-11 Nanophoton Corporation, Japan at 514 nm laser wavelength. The field emission scanning electron microscopy (FESEM) was performed on VEGA3, TESCAN (Czech Republic) and the parallel studies of energy dispersive X-ray analysis (EDX) was performed on BRUKER Nano, GmbH, D-12489 (Germany) (accelerating voltage of −0 to 30 KeV). For the drug estimation in drug release studies, the UV–Visible Diode array spectrophotometer on Agilent 8453 China-made instrument was employed.

3. Results and discussion

3.1. Physicochemical characterization

Fig. 1 shows the comparison of FTIR spectral peaks of various HAP samples as this technique provides information about the intermolecular bonding of typical HAP peaks at all combinations viz. (a) Pure HAP, (b) 2% FHAP, (c) 5% FHAP, (d) Cs-2% FHAP, and (e) Cs-5% FHAP. From the spectra, the broader peak observed at 3000 cm^{-1} attribute to the –OH stretching vibration, which denotes the adsorption of water available at the surface of apatite. Also, the peaks at 1096, 1048, and 961 cm^{-1} correspond to the stretching vibrations of the P–O bond [43,44]. Alongside, the bending vibrations of P–O was assigned to the peaks around 601, 532, and 430 cm^{-1} [40,45]. The characteristic peak of carbonate ion was observed at 1396 cm^{-1} in the apatite structure and found to be similar to the stoichiometry of HAP [40]. The detailed FTIR spectral peaks and corresponding bonding are provided in Table 2.

Fig. 2 shows the comparison of Raman spectral vibrations of (a) pure HAP, (b) 2% FHAP, (c) 5% FHAP, (d) Cs-2% FHAP, and (e) Cs-5% FHAP samples in the frequency range of 200–1200 cm^{-1}. From the graph, the Raman spectra provides a strong characteristic peak of tetrahedral PO_4 group (v_1) at 962 cm^{-1} as a dominant one and this corresponds to the symmetric P–O bond stretching. Also, the two v_3 (PO_4) peaks, single v_2 (PO_4), and v_4 (PO_4) peaks were resolved and could be assigned to the internal vibrational modes of phosphate groups [46,47].

The XRD profile of (a) pure HAP, (b) 2% FHAP, (c) 5% FHAP, (d) Cs-2% FHAP, and (e) Cs-5% FHAP were compared and provided in Fig. 3. The observed diffraction peaks are indicating the formation of all samples in their crystalline phases and in addition, the pure HAP sample diffraction can be indexed to the standard HAP (JCPDS card No: 09–0432), while all other diffraction patterns are relating to fluorapatite (JCPDS card No. 15–0876). From the comparison of reflection diffraction intensities, the peak intensity increases with that of the increased concentration of fluorine, but the difference was minimal. The diffraction peaks are observed at 26.1°, 29.2°, 32.0°, 33.2°, 34.3°, 40.0°, 46.9°, and 49.7° and these can be indexed to the planes of (002), (210), (211), (300), (202), (310), (222), and (213). Also, the comparison of crystallite sizes of all the samples are provided in Fig. 3(B) and Table 3, it can be worth mentioning that the crystallinity factor was increased with that of an increased concentration of dopant, i.e., the 5% FHAP sample was the highest crystal size of 55.8 nm, followed by the 2% FHAP (49.8 nm) and

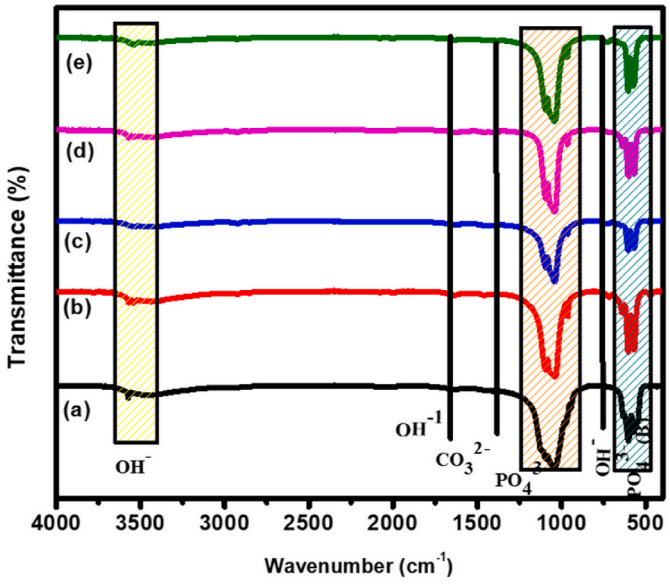

Fig. 1. FTIR spectral comparison of (a) pure HAP, (b) 2% FHAP, (c) 5% FHAP, (d) Cs-2% FHAP, and (e) Cs-5% FHAP.

Table 2
FTIR spectral analysis of as-prepared HAP sample.

Vibrational frequency (cm^{-1})	Peak assignments
3573	(υ_s) Stretching mode of HAP OH^- group
1634	(υ_2) OH^- bending mode of H_2O
1455	(υ_4 or υ_3) Bending mode of A & B type CO_3^{2-} group
1089	(υ_3) Asymmetric stretching mode of P–O bond of PO_4^{3-} group
1043	(υ_3) Asymmetric stretching mode of P–O bond of PO_4^{3-} group
964	(υ_1) Symmetric stretching mode of P–O bond of PO_4^{3-} group
715	(υ_1) in-plane bending vibration mode of OH
631	(υ_L) Liberational mode of OH^- a group of HAP
603	(υ_4) Bending mode of the O–P–O bond of the PO_4^{3-} group
571	(υ_4) Bending mode of the O–P–O bond of the PO_4^{3-} group
474	(υ_2) Bending mode of O–P–O bond of the PO_4^{3-} group

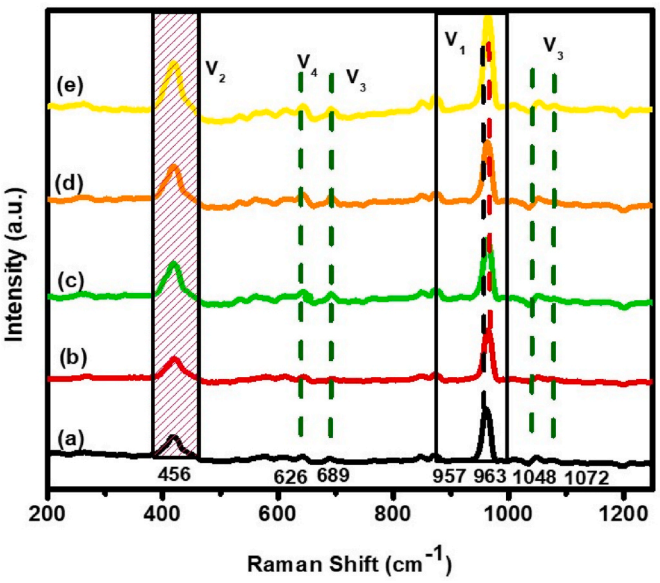

Fig. 2. Comparison of Raman spectral analysis of (a) pure HAP, (b) 2% FHAP, (c) 5% FHAP, (d) Cs-2% FHAP, and (e) Cs-5% FHAP.

so on. The following Debey-Scherrer relation provided in Eq. (5) was used to calculate the crystallite size of the particles.

$$D = \frac{0.9\lambda}{\beta \cos\theta} \quad (5)$$

Further, the XRD patterns also show that there was a moderate difference among the samples in terms of the relative intensity based on the diffraction planes (002), (211), and (300) for the five tested samples (Fig. 3B). This indicates the possibility of the formation of different preferential orientation growth for the FHAP crystals under different doping conditions.

Fig. 4 provides the surface morphological analysis of (a) pure HAP, (b) 2% FHAP, (c) 5% FHAP, (d) Cs-2% FHAP, and (e) Cs-5% FHAP where the electron micrograph of HAP shows the typical monodisperse and spherical shaped particles. Also, the EDX analysis of the same samples provided in Fig. 5 indicate the elemental peaks for the HAP sample related to P, Ca, and O with Ca/P in the ratio of 1.66. Further, the EDX analysis confirms the successful formation of the HAP and its associated composites of doping through the observation of peaks are related to the elements of Ca, P, C, O, and F. The elemental composition of HAP and FHAP samples are provided in Table 4.

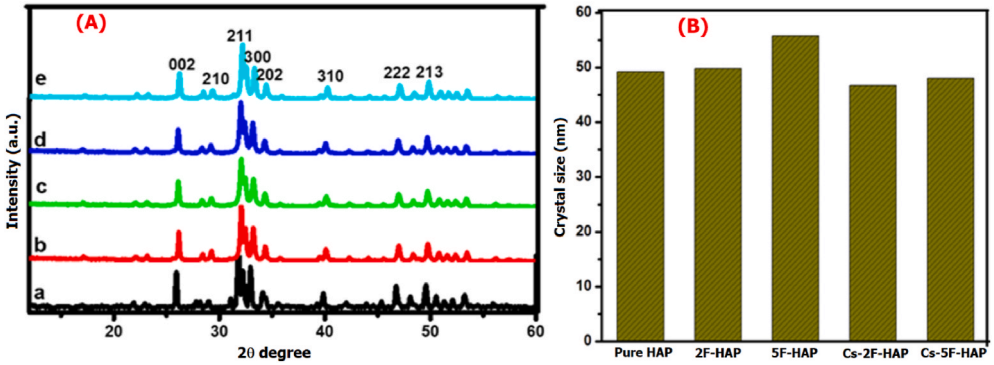

Fig. 3. Comparison of (A) powder XRD and (B) crystalline size analysis among the different samples of (a) pure HAP, (b) 2% FHAP, (c) 5% FHAP, (d) Cs-2% FHAP, (e) Cs-5% FHAP.

Table 3
Comparison of crystallite sizes of various HAP samples.

Samples	Crystallite size (nm)
Pure HAP	49.2
2% FHAP	49.8
5% FHAP	55.8
Cs-2% FHAP	46.7
Cs-5% FHAP	48.0

In the following step, the Cs-5% FHAP material was used for the formation of the composite scaffold with that of chitosan ad alginate. Fig. 6(a) shows the FTIR spectrum of as-prepared chitosan-alginate/5% FHAP scaffold composite where the sample exhibited characteristic bands around 3414, 2920, and 2859 cm^{-1}, corresponding to the stretching vibrations of N–H combined with –OH stretching vibration, while the band around 1632 cm^{-1} was the characteristic peaks of amide I and amide II, respectively. Also, the sharp peaks observed around 1425 cm^{-1} can be assigned to the CH_3 symmetrical deformation and the band at 1045 cm^{-1} corresponds to the C–O stretching vibrations (C–*O*–C). Similarly, the observation of FTIR peaks for the FHAP component in chitosan-alginate/5% FHAP composite scaffold around 1095, 965, 633, 604, and 567 cm^{-1} were found to be fully matching with that of FTIR analysis of pure FHAP nanocrystal (Fig. 1).

Fig. 6(b) shows the Raman spectrum of as-prepared chitosan-alginate/5% F-HAP composite scaffold and from the graph, the peak intensities related to 5% FHAP appeared to be minimal (as per Fig. 2). Such a decrease in the peak intensity of phosphate groups can be attributed to the masking of groups of organic moieties like chitosan and alginate. We investigated that the peaks observed at 599 and 623 cm^{-1} are corresponding to the phosphate groups and the shift in peak position from 961 to 965 cm^{-1} may be due to the F substitution and in that way, the 5% Fluorine substitution got confirmed. Also, the peaks observed at 1225, 1333, and 1548 cm^{-1} were due to the methyl group of alginate

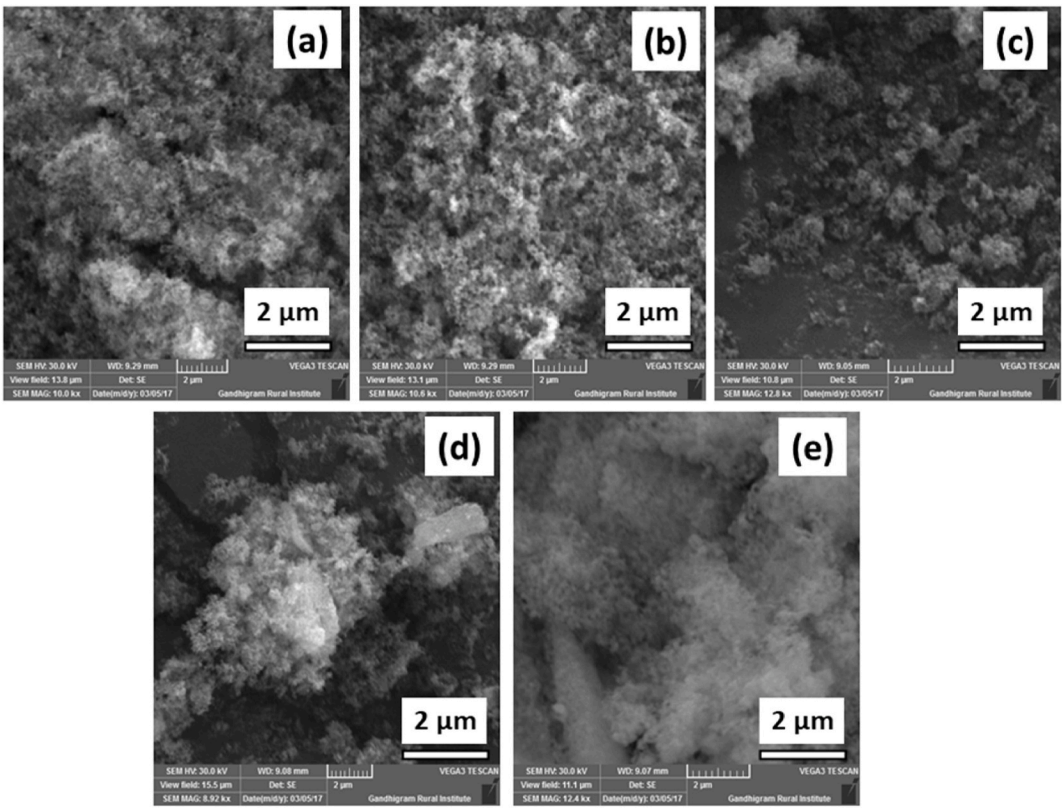

Fig. 4. FESEM images of (a) pure HAP, (b) 2% FHAP, (c) 5% FHAP, (d) Cs-2% FHAP, and (e) Cs-5% FHAP.

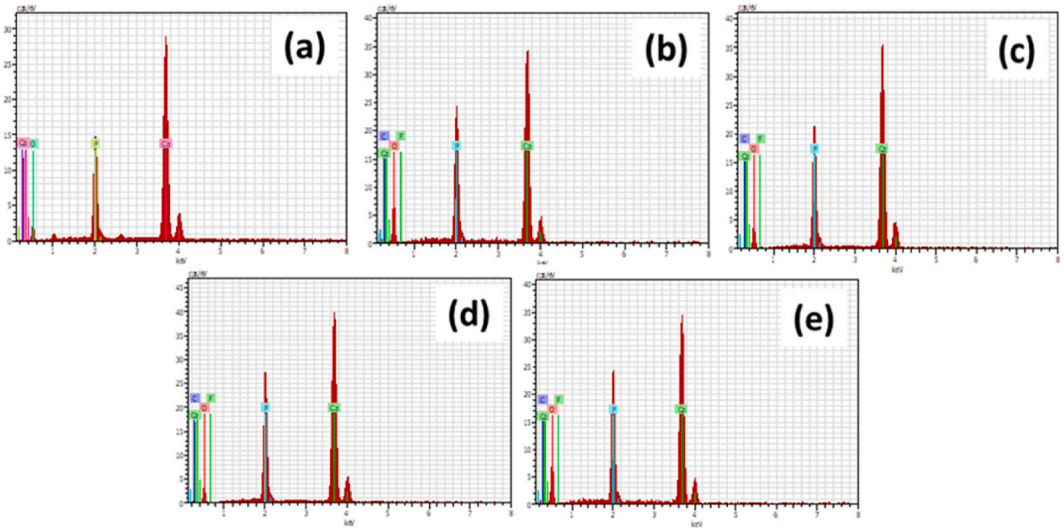

Fig. 5. EDAX analysis of (a) pure HAP, (b) 2% FHAP, (c) 5% FHAP, (d) Cs-2% FHAP, and (e) Cs-5% FHAP.

Table 4
The elemental composition of HAP and FHAP samples.

Sample	Ca (atomic %)	P (atomic %)	O (atomic %)	C (atomic %)	F (atomic %)
Pure HAP	23.41	14.25	54.32	3.11	0
2% FHAP	14.28	8.18	64.23	13.05	1.27
5% FHAP	26.38	14.40	51.57	7.15	3.52
Cs-2% FHAP	22.17	11.90	58.95	4.94	2.04
Cs-5% FHAP	21.42	10.90	56.36	8.00	4.32

and amide group of chitosan and all these analyses confirms the successful synthesis of chitosan-alginate/5% F-HAP composite scaffold.

The powder XRD patterns of as-prepared chitosan-alginate/5% F-HAP composite scaffold are provided in Fig. 6(c) and from the graph, the reflection patterns appear at 20.0° for chitosan and 26.1°, 29.2°, 32.0°, 33.2°, 34.3°, 40.0°, 46.9°, and 49.7° are relating to FHAP component. This analysis provides evidence for the successful synthesis of F-HAP crystals blended with the polymer matrix. However, the broad peaks and crystallinity of FHAP were observed. This decreased intensity of peaks and crystallinity can be due to the masking of FHAP crystals by the organic moieties used during the scaffold preparation.

The morphological features of the chitosan-alginate/5% FHAP scaffold composite are provided in Fig. 6(d) and from the image, the formation of uniform pores with the presence of FHAP mineral phases within the polymer matrix has observed. This leads to the generation of a more compact structure that supports fully the incorporation of drugs, genes, or other therapeutic agents for sustained and targeted release.

3.2. Studies of bioactivity and drug release

The *in vitro* bioactivity tests were performed for the pure HAP and 2% FHAP, 5% FHAP, Cs-2% FHAP, and Cs-5% FHAP samples, and investigated based on the formation of apatite layer at the surface of the sample. For testing, the samples were pelletized and immersed in the SBF for 21 days at 37 °C as mentioned earlier and recorded the changes in morphological features by making use of the FESEM (as provided in Fig. 7). The growth of the apatite layer onto the surface of tested HAP samples involves their dissolution and subsequent precipitation of the formed apatite. After the immersion of samples into the dissolution medium, the samples get dissolved. With an increase of immersion period, the dissolution rate and precipitation rate also increases. This process continued until the solution reaches an equilibrium where the Ca and P concentrations become saturated, i.e., HAP attains a negative surface charge while the phosphate and hydroxyl groups are present at the surface. Since, the SBF medium contains the positively charged calcium ions and, in that way, the positive ions get interacted with the negatively charged ions of HAP, which results in Ca-rich amorphous calcium phosphate (Ca-rich ACP) with the production of positive surface charges. These positively charged Ca-rich ACP gets interacted with the negatively charged phosphate ions available in the SBF medium to generate Ca-deficient ACP and that's why the SBF causes the growth of bone-like apatite.

Fig. 8 shows the bioactivity of the chitosan-alginate/5% FHAP scaffold acquired using SEM micrographs for the sample after immersion in SBF at 37 °C for 7 days. It can be observed from the image that the scaffold sample after its incubation in SBF solution seems to develop the formation of an apatite layer over its surface. This involves a sequence of events including the release of ions from FHAP followed by the resorption, nucleation, and subsequent growth of calcium phosphate, as revealed by the EDX with the peaks observed from the elements of P, Ca, and O.

Fig. 9 shows the comparison of CIP drug release behaviour of (a) pure HAP, (b) 2% FHAP, (c) 5% FHAP, (d) Cs-2% FHAP, and (e) Cs-5% FHAP samples under *in vitro* conditions (PBS; pH 7.4) and the optical absorption as a function of time was measured. From the graph, it can be observed that the pure HAP exhibits an initial burst release of ~49% of the loaded CIP drug and in contrast, all the other FHAP samples showed a relatively lower extent of CIP drug burst release. However, for the other samples of F-substituted HAP, the percentage of CIP release seems to be strongly influenced by the fluorine amount and Cs-micelle used for the formation of FHAP nanocomposites. We observed that the sample with a higher concentration of fluorine, the CIP release (%) was low with steady rate. Since the remnant, Cs was removed during the sintering process performed at 800 °C temperature for 2 h and so, a decrease in size can be expected with the micelle-assisted sample that contributes to the nanostructure. Such an organization of size reduction for the nanostructures was found to be consistent with morphological analyses as observed from the FESEM (Fig. 8).

The results provided in Fig. 9 indicate that the sintered pure HAP sample has released about 92.08% of its loaded drug during the first 70 min and with the initial burst of release that accounts for 49%. However, the other samples over a 80 min period has the drug release of 87.68% (2% FHAP), 85.47% (5% FHAP), 78.46% (Cs-2% FHAP), and 70.30% (Cs-5% FHAP). Among the sintered samples, the observed differences in drug release behaviour with respect to time can be attributed to the

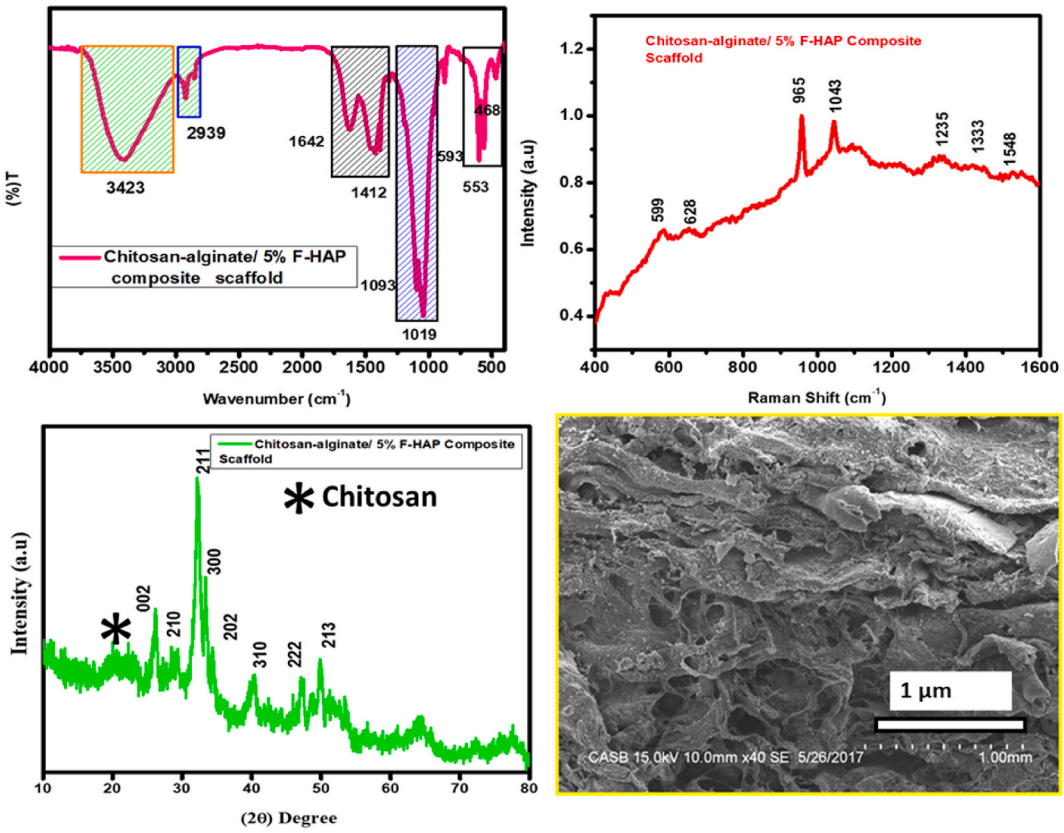

Fig. 6. FTIR, Raman, XRD, and SEM for chitosan-alginate/5% FHAP composite scaffold.

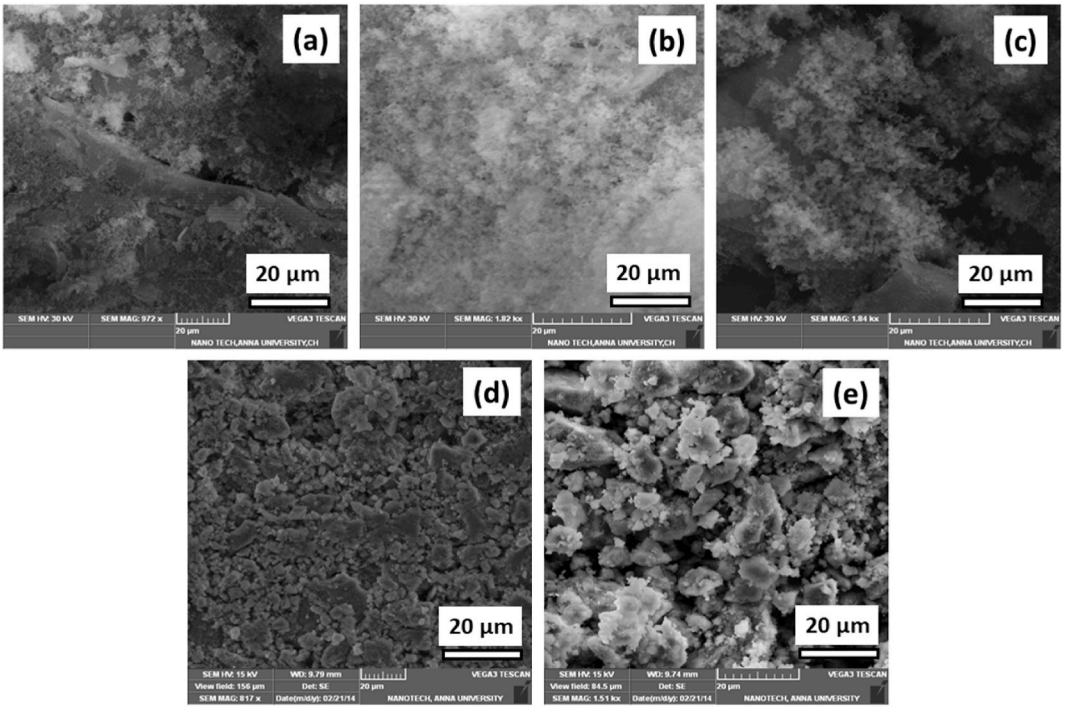

Fig. 7. FESEM images of (a) pure HAP, (b) 2% FHAP, (c) 5% FHAP, (d) Cs-2% FHAP, and (e) Cs-5% FHAP.

formation of different-sized crystalline particles followed by the removal of Cs-moiety in the sintering process. The formation of micelles by the Cs moieties around the Cs-2% FHAP and Cs-5% FHAP crystallites, result in a size reduction which helps to control the drug release behaviour. Within the nanocomposites, this variation in the drug release behaviour are due to the size effects, creating a novel path for the transportation and release of the loaded drug to the targeted sites.

Similarly, Fig. 10 shows the drug release profile from the chitosan-

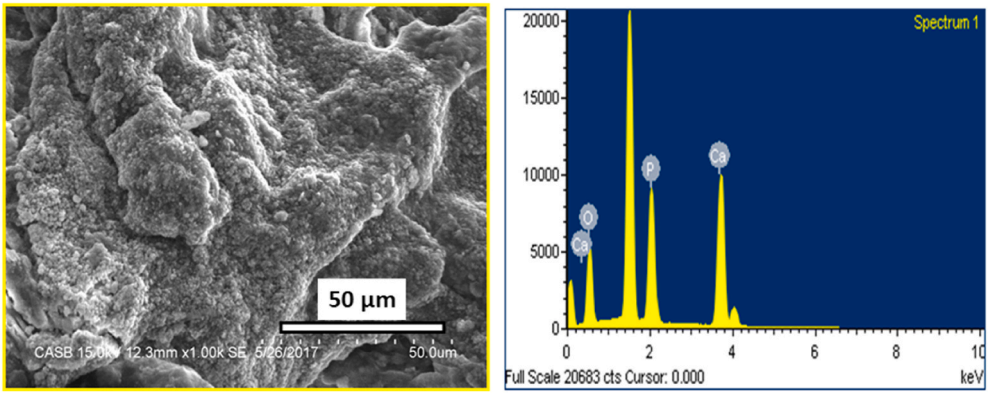

Fig. 8. FESEM provided bioactivity and the corresponding EDX analysis for the chitosan-alginate/5% FHAP scaffold composite.

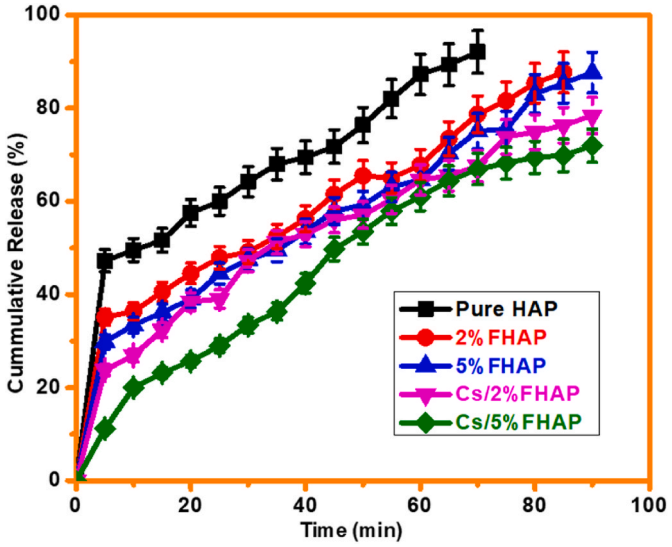

Fig. 9. Cumulative drug release studies of (a) pure HAP, (b) 2% FHAP, (c) 5% FHAP, (d) Cs-2% FHAP, and (e) Cs-5% FHAP.

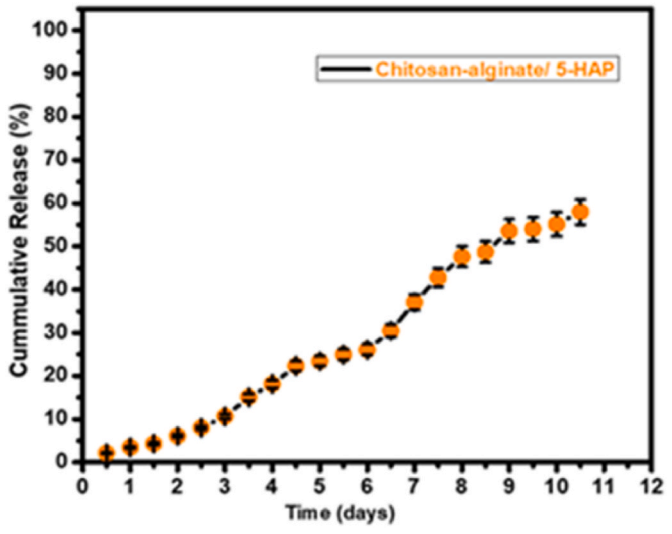

Fig. 10. CIP drug release profile of chitosan-alginate/5% F-HAP scaffold composite.

alginate/5% FHAP carrier. The CIP antibiotic drug was loaded by the immersion into the PBS (pH 7.4) where the release was quantified by taking the optical absorption as a function of time. From the graph, the scaffold exhibits the total CIP release of 60% during the tested period of 11 days and the release profile appeared to be slow and very much controlled. Such an observation of slow CIP release can be linked to the bonding of drug with that of chitosan-alginate matrices and at the same time, the strong affinity of drug molecules towards the negative ions of fluorine brings the delivery to be controlled. From the results of chitosan-alginate/5% F-HAP composite, it shows suitable carrier for the controlled release of drugs for prolonged time periods.

3.3. Measurement of porosity, water uptake and retention ability

The porosity of the chitosan-alginate/5% FHAP scaffold sample was calculated using the following formula,

$$\text{Porosity} = (V_1 - V_3) / (V_2 - V_3) \times 100 \quad (6)$$

Where V_1 is the initial known weight of scaffold, V_2 is the sum of weights of ethanol and submerged scaffold, and V_3 is the weight of ethanol after the scaffolding removal.

Since, porosity is an important parameter to assess the capacity of any scaffold material for bone tissue engineering applications. It preserves the tissue volume, with temporary mechanical function, facilitates cell migration, and deliver the protein to cells. The porosity studies performed on chitosan-alginate/5% FHAP scaffold are compared with that of chitosan/5% FHAP and shown in Fig. 11(a). From the results, noticed that the porosity of chitosan-alginate/5% F-HAP (88.78%) are slightly lesser than chitosan/5% F-HAP scaffold (92.87%). Such a decrease in the total porosity of the tri-component scaffolds system as compared to the bi-component suggesting for the occurrence of possible chemical interactions through the involvement of alginate. In general, it is considered to have a scaffold with 90% porosity as sufficient for cell attachment and proliferation purposes. The scaffolds formed by the freeze-drying technique usually have better pore sizes as compared to the scaffolds prepared by any other technique like sol-gel, co-precipitation etc.

The percentage of water absorption (E_A) and water retention (E_R) for the prepared chitosan-alginate/5% FHAP scaffold was calculated using the following formulae.

$$E_A = [(W_{wet} - W_{dry}) / W_{dry}] \times 100 \quad (7)$$

$$E_R = [(W'_{wet} - W_{dry}) / W_{dry}] \times 100 \quad (8)$$

W' – the weight of wet scaffold after centrifugation.

In general, for any scaffold used for biomedical and bioengineering applications, understanding the water uptake and retention ability are very much essential to complete analyze the absorption of physiological

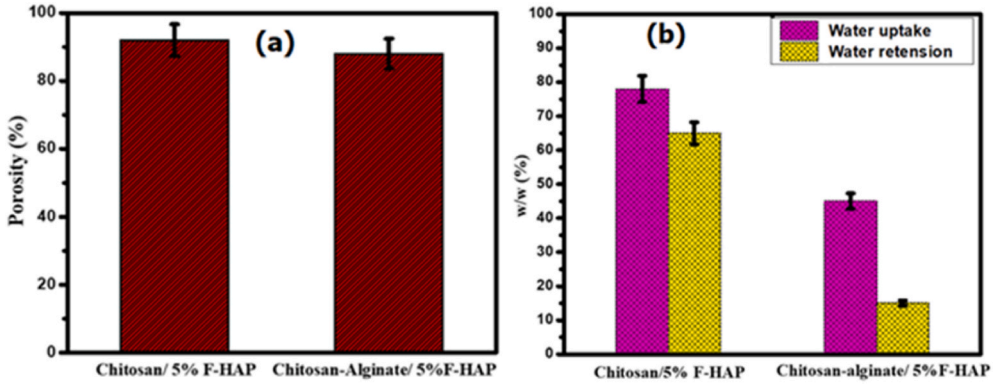

Fig. 11. (a) Porosity, and (b) water uptake and retention studies of chitosan-alginate/5% FHAP scaffold composite.

fluids and associated transfer of nutrients, metabolites through the scaffolds. Fig. 11(b) provides the water uptake and retention ability of as-prepared chitosan-alginate/5% FHAP scaffold compared with that of chitosan/5% FHAP scaffold. It can be noted from the results, that the chitosan-alginate/5% FHAP scaffold has less water uptake and retention ability in relation to the chitosan/5% FHAP scaffold. We calculated that the water uptake and retention (%) for chitosan/5% F-HAP are 78 and 45%, while for the chitosan-alginate/5% FHAP are 65 and 15%. Interestingly, the inclusion of alginate polysaccharides in the chitosan composite are decreasing the degree of water absorption of chitosan-alginate/5% FHAP. However, the chitosan-alginate/5% FHAP composite scaffold has the water uptake and retaining ability, that is sufficient enough for the maintenance of metabolite flow for the growth of bones.

3.4. *In vitro* biodegradation and antimicrobial studies

Fig. 12 shows the *in vitro* biodegradation studies of chitosan-alginate/5% F-HAP composite compared with that of chitosan/5% F-HAP composite and for the analysis, the weight loss (W_L) was calculated as per the following formula,

$$W_L = [(W_0 - W_1)/W_0] \times 100\% \quad (9)$$

Where, W_0 and W_1 denotes the weights of samples before and after soaking, respectively.

From the biodegradation study over the testing period of 21 days, it was found that the chitosan/5% FHAP composite got degrade around 67.5% of its original weight and high, as compared to the chitosan-alginate/5% F-HAP scaffold degradation (only 58.3%). The observation of limited biodegradation for the chitosan-alginate composite can be attributed to the presence of a tri-component system in the composite. This controllable biodegradation of the scaffold can be suitable for bone engineering applications to withstand the mechanical stresses and provide a suitable surface for cell attachment and growth. Also, the slow and controlled degradation supports well for sustainability by playing the materials as a crucial role in the long-term performance of transplanted bone tissues. Since, easily degradable biopolymeric scaffolds maintain the nominal mechanical properties, they can also easily absorbed by the body with no traces left. Thus, the controlled degradation behaviour are mostly by the availability of alginate as chitosan component which are hydrolytically unstable material and it accelerates with the degradation in an aqueous medium.

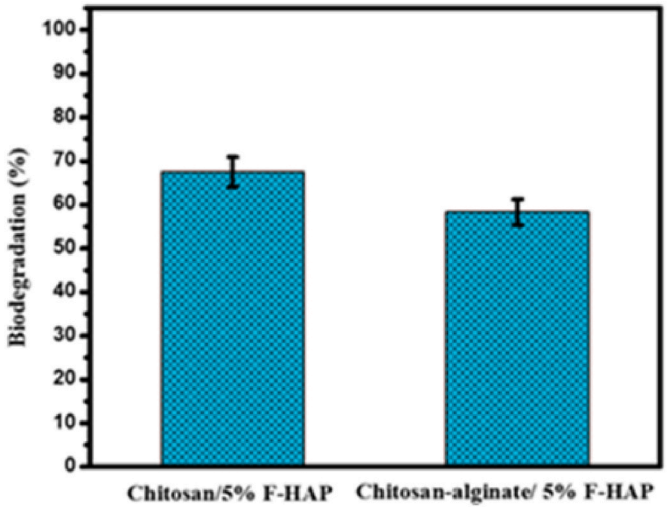

Fig. 12. Biodegradation studies of chitosan/5% F-HAP and chitosan-alginate/5% F-HAP scaffold composite.

The antimicrobial activity for the three different HAP samples of H1, H2, and H3 were performed and the results shown in Fig. 13 and quantitatively in Tables 5 and 6. From the quantitative analysis results measured using ZoI, it can be mentioned that the Cs-5% FHAP sample has the highest antibacterial activity as compared to the Cs-2% FHAP and pure HAP samples. Within the two bacterial cultures tested, the highest activity was noted against the gram-positive bacteria with the ZoI of 47 mm, followed by the gram-negative bacteria with 38 mm ZoI. Further, the antifungal activity seems to have no difference among the two samples of H2 and H3, and the ZoI was observed for both, and found to be better than that of H1 sample (pure HAP). This analysis provides the information that the FHAP samples are maintaining the antimicrobial (antibacterial and antifungal) activity in a better proportion than that of pure HAP samples and thereby providing evidence for the importance of forming fluorine substituted HAP composite.

4. Conclusion

In conclusion, we confirm the suitable characteristics of chitosan-alginate/5% FHAP scaffold composite for the biomedical sectors particularly suitable for the orthopaedic applications of bone tissue growth and replacement. Various HAP composites were synthesized with two different F content and composition. The 5% FHAP were formed from the Cs micelle assisted approach (Cs-5% FHAP). It is found to be stable and efficient, in terms of crystallinity, morphology, bioactivity, and with the controlled CIP drug release behavior. Also, the scaffolds formed from chitosan-alginate/5% FHAP (as compared to pure Cs-5% FHAP composite) has the superior characteristics of porosity (88.78%), water uptake (65%), water retention (15%), biodegradation capacity (67.5% in 21 days), along with the controlled CIP release ability (60% in 11 days). Further, the antibacterial activity tests were conducted against *Staphylococcus aureus* (ZoI of 47 mm) and *Escherichia coli* (ZoI of 38 mm), and antifungal activity against *Candida albicans* (ZoI of 10 mm) confirmed the biological efficacy of Cs-5% FHAP composite.

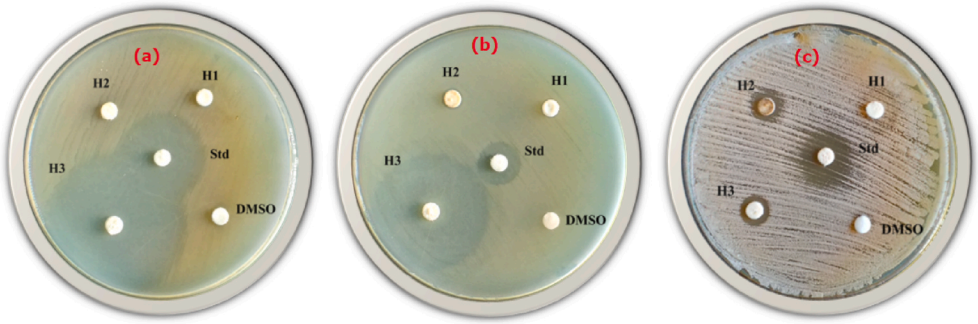

Fig. 13. Analysis of the biological activity of the tested samples (H1-pure HAP, H2–Cs-2% FHAP, and H3–Cs-5% FHAP) towards (a) *Staphylococcus aureus*, (b) *Escherichia coli*, and (c) *Candida albicans*.

Table 5
ZoI observed for the antibacterial activity.

Microorganism	ZoI (mm)				
	H1	H2	H3	DMSO	S
Staphylococcus aureus	8 ± 2	–	47 ± 2.2	–	27 ± 1.3
Escherichia coli	6.5 ± 1.8	7 ± 1.5	38 ± 2	–	14 ± 1.7

Table 6
ZoI observed for the antifungal activity.

Microorganism	ZoI (mm)				
	H1	H2	H3	DMSO	K
Candida albicans	–	10 ± 0.5	10 ± 0.7	–	18 ± 0.5

The cumulative analysis of result shows that the as-synthesized chitosan-alginate/5% FHAP composite prepared from the Cs micelle mediated synthesis can be suitable for biomedical applications of orthopaedic implants.

CRediT authorship contribution statement

S.A. Iynoon Jariya: Conceptualization, Methodology, Formal analysis, Writing – original draft. **Varun Prasath Padmanabhan:** Methodology, Formal analysis, Data curation, Visualization, Validation. **Ravichandran Kulandaivelu:** Supervision, Formal analysis, Data curation, Visualization, Validation. **Natarajan Prakash:** Formal analysis, Validation, Data curation. **Faruq Mohammad:** Investigation, Formal analysis, Data curation, Visualization, Validation. **Hamad A. Al-Lohedan:** Data curation, Visualization, Validation. **Suriati Paiman:** Data curation, Visualization, Validation. **Romana Schirhagl:** Data curation, Visualization, Validation. **M.A. Motalib Hossain:** Formal analysis, Data curation, Visualization, Validation. **Suresh Sagadevan:** Formal analysis, Data curation, Validation, Writing – review & editing.

Declaration of competing interest

The authors declare that they have no known competing financial interests or personal relationships that could have appeared to influence the work reported in this paper.

Acknowledgement

S. A. Iynoon Jariya acknowledges the Department of Science and Technology (DST), India for the financial support in the form of Junior Research Fellowship (IF150141) under the DST-INSPIRE program. One of the authors Varun Prasath Padmanabhan most sincere gratitude to the Council of Scientific and Industrial Research (CSIR), Government of India, for financial support in the form of Research Associate Fellowships (09/115(0793)/2020-EMR-I.

References

[1] S.K. Bhullar, D.G. Ruzgar, S. Saber-Samandari, M. Sadighi, S. Ahadian, M. Ramalingam, Impact of nanophase hydroxyapatite-based biomaterials on tissue engineering, J. Bionanoscience 12 (2018) 469–477.
[2] Anita Lett, Suresh Sagadevan, Is Fatimah, et al., Recent advances in natural polymer-based hydroxyapatite scaffolds: properties and applications, Eur. Polym. J. 148 (2021) 110360.
[3] V.P. Padmanabhan, Ravichandran Kulandaivelu, et al., Influence of sonication on the physicochemical and biological characteristics of selenium-substituted hydroxyapatites, New J. Chem. 44 (2020) 17453–17464.
[4] Subha Balakrishnan, et al., Influence of iron doping towards the physicochemical and biological characteristics of hydroxyapatite, Ceram. Int. 47 (2021) 5061–5070.
[5] Anita Lett, et al., Tailoring the morphological features of sol-gel synthesized mesoporous hydroxyapatite using fatty acids as an organic modifier, RSC Adv. 9 (2019) 6228–6240.
[6] S. Saber-Samandari, N. Nezafati, S. Saber-Samandari, The effective role of hydroxyapatite based composites in anticancer drug delivery systems, Crit. Rev. Ther. Drug Carrier Syst. 33 (2016) 41–75.
[7] Anita Lett, Y. Y Sivaram, Bala Manikanta et al, Biocompatible silver incorporated hydroxyapatite; synthesis, characteristics for biomedical application, AIP Conference Proceedings 2311 (2020), 080010.
[8] V.P. Padmanabhan, et al., Drug delivery and in vitro biological effects of gum ghatti-modified hydroxyapatite nanoporous composites, Mater. Chem. Phys. 263 (2021) 124385.
[9] S.V. Dorozhkin, Multiphasic calcium orthophosphate ($CaPO_4$) bioceramics and their biomedical applications, Ceram. Int. 42 (2016) 6529–6554.
[10] V.P. Padmanabhan, et al., Nanoformulations of core–shell type hydroxyapatite-coated gum acacia with enhanced bioactivity and controlled drug delivery for biomedical applications, New J. Chem. 44 (2020) 7175–7185.
[11] A. Lett, S. Sagadevan, G.S. Kaliaraj, K. Alagarsamy, et al., Synthesis, characterization, and electrical properties of alkali earth metal-doped bioceramics, Mater. Chem. Phys. 249 (2020) 123–141.
[12] J. Anita Lett, Suresh Sagadevan, J. Joyce Prabhakar, M. Bavani Latha, Exploring the binding effect of a seaweed-based gum in the fabrication of hydroxyapatite scaffolds for biomedical applications, Mater. Res. Innovat. 24 (2019) 1–7.
[13] V.P. Padmanabhan, R. Kulandaivelu, et al., Facile fabrication of phase transformed Cerium (IV) doped Hydroxyapatite for biomedical applications - a health care approach, Ceram. Int. 46 (2020) 2510–2522.
[14] V.P. Padmanabhan, R. Kulandaivelu, D.S. Panneer, et al., Surfactant assisted hydroxyapatite nanoparticles: drug loading and in vitro leaching kinetics and antimicrobial properties, J. Nanosci. Nanotechnol. 19 (2019) 7198–7204.
[15] J. Anita Lett, M. Sundareswari, K. Ravichandran, Bavani Latha, Suresh Sagadevan, Fabrication and characterization of porous scaffolds for bone replacements using gum tragacanth, Mater. Sci. Eng. C 96 (2019) 487–495.
[16] D. Brasinika Tsetsekou, V. Vaou, E. Chatzitheodoridis, On the synthesis of tailored biomimetic hydroxyapatite nanoplates through a bioinspired approach in the presence of collagen or chitosan and L-arginine, Mater. Sci. Eng. C 43 (2014) 555–565.
[17] Varun Prasath Padmanabhan, Ravichandran Kulandaivelu, Sankara Narayanan T. S. Nellaiappan, New core-shell hydroxyapatite/gum-acacia nanocomposites for drug delivery and tissue engineering applications, Mater. Sci. Eng. C 92 (2018) 685–693.
[18] Feng Ye, Haifeng Guo, Haijiao Zhang, Xiulan He, Polymeric micelle-templated synthesis of hydroxyapatite hollow nanoparticles for a drug delivery system, Acta Biomater. 6 (2010) 2212–2218.
[19] Li Junjie, Yi Ping Chen, Yuji Yin, Yao Fanglian, Yao Kangde, Modulation of nano-hydroxyapatite size via formation on chitosan–gelatin network film *in situ*, Biomaterials 28 (2007) 781–790.

[20] S. Saber-Samandari, S. Saber-Samandari, F. Ghonjizade-Samani, J. Aghazadeh, A. Sadeghi, Bioactivity evaluation of novel nanocomposite scaffolds for bone tissue engineering: the impact of hydroxyapatite, Ceram. Int. 42 (2016) 11055–11062.
[21] J.M. Coelho, J. Agostinho Moreira, A. Almeida, F.J. Monteiro, Synthesis and characterization of HAp nanorods from a cationic surfactant template method, J. Mater. Sci. Mater. Med. 21 (2010) 2543–2549.
[22] Pakvipar Chaopanich, Punnama Siriphannon, Facile refluxing synthesis of hydroxyapatite nanoparticles, Aust. J. Chem. 68 (2015) 1293–1298.
[23] Y. Liu, D. Hou, G. Wang, A simple wet chemical synthesis and characterization of hydroxyapatite nanorods, Mater. Chem. Phys. 86 (2004) 69–73.
[24] M. Zolghadri, S. Saber-Samandari, S. Ahmadi, et al., Synthesis and characterization of porous cytocompatible scaffolds from polyvinyl alcohol–chitosan, Bull. Mater. Sci. 42 (2019) 35.
[25] A. Fahami, B.N. Tabrizi, R.E. Kahrizsangi, Synthesis of calcium phosphate-based composite nanopowders by mechanochemical process and subsequent thermal treatment, Ceram. Int. 38 (2012) 6729–6738.
[26] Carlos García, Claudia García, Carlos Paucar, Controlling morphology of hydroxyapatite nanoparticles through hydrothermal microemulsion chemical synthesis, Inorg. Chem. Commun. 20 (2012) 90–92.
[27] Anita Lett, et al., Exploring the thumbprints of Ag-hydroxyapatite composite as a surface coating bone material for the implants, J. Mater. Res. Technol. 9 (2020) 12824–12833.
[28] V. Asadian-Ardakani, S. Saber-Samandari, S. Saber-Samandari, The effect of hydroxyapatite in biopolymer-based scaffolds on release of naproxen sodium, J. Biomed. Mater. Res. A. 104 (2016) 2992–3003.
[29] B.H. Chen, K.I. Chen, M.L. Ho, H.N. Chen, W.C. Chen, C.K. Wang, Synthesis of calcium phosphates and porous hydroxyapatite beads prepared by emulsion method, Mater. Chem. Phys. 113 (2009) 365–371.
[30] S. Saber-Samandari, K. Alamara, S. Saber-Samandari, Calcium phosphate coatings: morphology, micro-structure and mechanical properties, Ceram. Int. 40 (2014) 563–572.
[31] D. Gopi, N. Bhuvaneshwari, J. Indira, K. Kanimozhi, L. Kavitha, A novel green template-assisted synthesis of hydroxyapatite nanorods and their spectral characterization, Spectrochim. Acta A Mol. Biomol. Spec. 107 (2013) 196–202.
[32] M. Hadavi, S. Hasannia, S. Faghihi, F. Mashayekhi, H. Zadeh, S. Mostofi, Novel calcified gum Arabic porous nano-composite scaffold for bone tissue regeneration, Biochem. Biophys. Res. Commun. 488 (2017) 671–678.
[33] C. Zhang, C. Li, S. Huang, Z. Hou, Z. Cheng, P. Yang, C. Peng, J. Lin, Self-activated luminescent and mesoporous strontium hydroxyapatite nanorods for drug delivery, Biomaterials 31 (2010) 3374–3383.
[34] Y.-H. Liang, C.-H. Liu, S.-H. Liao, Y.-Y. Lin, H.-W. Tang, S.-Y. Liu, I.-R. Lai, K.C.-W. Wu, Cosynthesis of cargo-loaded hydroxyapatite/alginate core-shell nanoparticles (HAP@Alg) as pH-responsive nano vehicles by a pre-gel method, ACS Appl. Mater. Interfaces 4 (2012) 6720–6727.
[35] C. Felgines, O. Texier, C. Morand, C. Manach, A. Scalbert, F. Régerat, C. Rémésy, Bioavailability of the flavanone naringenin and its glycosides in rats, Am. J. Physiol. Gastrointest. Liver Physiol. 279 (2000) G1148–G1154.
[36] A. Jenifer, et al., Investigation on antibacterial and hemolytic properties of magnesium-doped hydroxyapatite nanocomposite, Chem. Phys. Lett. 771 (2021) 138539.
[37] R. Vani, E. Girija, K. Elayaraja, S.P. Parthiban, R. Kesavamoorthy, S.N. Kalkura, Hydrothermal synthesis of porous triphasic hydroxyapatite/(α and β) tricalcium phosphate, J. Mater. Sci. Mater. Med. 20 (2009) 43–48.
[38] K. Blakeslee, R.A. Condrate, Vibrational spectra of hydrothermally prepared hydroxyapatites, J. Am. Ceram. Soc. 54 (1971) 559–563.
[39] B. Sreedhar, D.K. Devi, A.S. Neetha, V.P. Kumar, K. Chary, Green synthesis of gum-acacia assisted gold-hydroxyapatite nanostructures–characterization and catalytic activity, Mater. Chem. Phys. 153 (2015) 23–31.
[40] V. Sarath Chandra, G. Baskar, R. Suganthi, K. Elayaraja, M. Ahymah Joshy, W. Sofi Beaula, R. Mythili, G. Venkatraman, S. Narayana Kalkura, Blood compatibility of iron-doped nanosize hydroxyapatite and its drug release, ACS Appl. Mater. Interfaces 4 (2012) 1200–1210.
[41] E. Győri, I. Fábián, I. Lázár, Effect of the chemical composition of simulated body fluids on aerogel-based bioactive composites, J. Compos. Sci. 15 (2017) 1–12.
[42] L.F. Sukhodub, L.B. Sukhodub, O. Litsis, Y. Prylutskyy, Synthesis and characterization of hydroxyapatite-alginate nanostructured composites for the controlled drug release, Mater. Chem. Phys. 217 (2018) 228–234.
[43] R. Vani, E. Girija, K. Elayaraja, S.P. Parthiban, R. Kesavamoorthy, S.N. Kalkura, Hydrothermal synthesis of porous triphasic hydroxyapatite/(α and β) tricalcium phosphate, J. Mater. Sci. Mater. Med. 20 (2009) 43–48.
[44] W.P. Griffith, Raman studies on rock-forming minerals. Part II. Minerals containing MO_3, MO_4, and MO6 groups, J. Chem. Soc. A (1970) 286–291.
[45] P.N. de Aza, F. Guitian, C. Santos, S. de Aza, R. Cusco, L. Artus, Vibrational investigation of calcium phosphate compounds. 2. Comparison between hydroxyapatite and β-tricalcium phosphate, Chem. Mater. 9 (1997) 916–922.
[46] Wolfgang Jahnke, Chrystele Henry, An *in vitro* assay to measure targeted drug delivery to bone mineral, ChemMedChem 5 (2010) 770–776.
[47] G.V. Radha, T. Sudha Rani, B. Sarvani, A review on proniosomal drug delivery system for targeted drug action, J. Basic Clin. Pharm. 4 (2) (2013) 42–48.